



Discussion

Automatic window size selection in Windowed Fourier Transform for 3D reconstruction using adapted mother wavelets

Sergio Fernandez ^{a,*}, Munther A. Gdeisat ^b, Joaquim Salvi ^a, David Burton ^b

^a Institute of Informatics and Applications, University of Girona, Av. Lluís Santalo S/N, E-17071 Girona, Spain

^b The General Engineering Research Institute (GERI), Liverpool John Moores University, James Parsons Building Room 114, Byrom Street, Liverpool L3 3AF, United Kingdom

ARTICLE INFO

Article history:

Received 10 November 2010

Received in revised form 21 December 2010

Accepted 25 January 2011

Available online 12 February 2011

Keywords:

Coded patterns

Pattern projection

Structured light

Fourier Transform

Windowed Fourier Transform

Wavelet Transform

3D measuring devices

Active stereo

Computer vision

ABSTRACT

Fringe pattern analysis in coded structured light constitutes an active field of research. Techniques based on first projecting a sinusoidal pattern and then recovering the phase deviation permit the computation of the phase map and its corresponding depth map, leading to a dense acquisition of the measuring object. Among these techniques, the ones based on time-frequency analysis permit to extract the depth map from a single image, thus having potential applications measuring moving objects. The main techniques are Fourier Transform (FT), Windowed Fourier Transform (WFT) and Wavelet Transform (WT). This paper first analyzes the pros and cons of these three techniques, then a new algorithm for the automatic selection of the window size in WFT is proposed. This algorithm is compared to the traditional WT using adapted mother wavelet signals both with simulated and real objects, showing the performance results for quantitative and qualitative evaluations of the new method.

© 2011 Elsevier B.V. All rights reserved.

1. Introduction

Among the vast contribution of Coded Structured Light (CSL) produced in the last decades, applications requiring dense acquisition with real-time response have experienced a recent increase due to the necessity to measure moving objects. Former techniques were based on fast capturing cameras capturing a set of time-multiplexed patterns [1,2]. However, the ability to measure moving objects regardless of the speed of motion (up to the acquisition time required by the camera) is only achieved by one-shot techniques. Latter, different techniques based on De Bruijn sequences and M-arrays were developed [3–6], obtaining a sparse acquisition with absolute coding and good accuracy results (despite some errors may arise in noisy areas due to code perturbation). Still, dense acquisition is only achieved by projecting a pattern or a set of patterns having continuous variation among at least one direction in the projection coordinates. Some techniques projected a grayscale pattern or a rainbow pattern coded in the spatial domain, which are the case of the patterns proposed by Carrhill and Hummel [7] and Tajima and Iwakawa [8], respectively, though both suffer from low resistance to noise and low level of accuracy [9]. A solution was given by fringe-based optical metrology. In fringe analysis one or more sinusoidal patterns are projected onto the scene. The deformation caused by the 3D shape is reflected in the phase

deviation (discrepancy between the projected and the imaged pattern). Extracting the phase, the 3D shape of the measuring scene can be obtained. There are five different techniques used traditionally for phase extraction: Phase Measurement Profilometry (PMP), Spatial Phase Detection (SPD), Fourier Transform (FT), Windowed Fourier Transform (WFT) and Wavelet Transform (WT). Among them, only SPD those based on frequency analysis (FT, WFT and WT) project one single shot and thus are able to work with moving objects. Regarding these frequency-based techniques, the main differences among them are related to the section of the imaged pattern that is considered in the frequency analysis. FT performs a global analysis, which is appropriate for stationary signals with poor spatial localization. However, this is not the case in CSL, which is by nature limited in space and thus non-stationary. This fact led to the use of the other two frequency based transforms (WFT and WT), which analyze local information in the imaged pattern. WFT and WT are constituted by two main steps: windowing the imaged pattern in local patches and computing the transform at every local patch. The crucial point in these techniques relies on the necessity of selecting an optimal window size, which constitutes a trade-off between resolution in space and resolution in frequency. In this work, a new proposal on the use of WFT is presented, where an algorithm for the automatic selection of the window size is proposed. Moreover, as it is not possible to find in the literature a study of windowing signals assuring good results for fringe pattern analysis using WFT, the adaption of four well known mother wavelet (Morlet, Paul, Shannon and Spline) is applied to WFT in order to compare the proposed

* Corresponding author.

E-mail address: sergiofn@eia.udg.edu (S. Fernandez).

algorithm for WFT with the WT. Finally, some results and comparison with classical WT are shown.

The paper is structured as follows: Section 2 presents a brief overview on dense acquisition methods, while Section 3 performs an analytical comparison of WFT versus WT techniques. Section 4 proposes a novel algorithm for the automatic selection of the window. Section 5 shows quantitative and qualitative results obtained with both simulated and real data for the four different mother wavelets. Finally, Section 6 states the conclusions, pointing out the suitability of the four mother wavelets employed in the tests and their performance in comparison to the traditional WT.

2. Overview of dense acquisition techniques

Dense acquisition in CSL refers to the ability to obtain a full-resolution acquisition of the measured scene, assuming that a continuous pattern is projected. Continuous patterns (also continuous coding strategies) show a continuous intensity or color variation along the coding axis [10]. Different continuous approaches have been proposed in the literature, the majority of them using a fringe pattern with trapezoidal or sinusoidal shapes. Among them, sinusoidal strategies present lower errors due to defocusing [1] and are easier to analyze by means of a transformation to the frequency domain. The 3D information of the scene is contained in the phase deviation of the sinusoidal fringe, which is extracted using a phase extraction algorithm. Some of the phase extraction approaches present in the literature are, chronologically, Phase Measurement Profilometry (PMP), Fourier Transform (FT), Spatial Phase Detection (SPD), Windowed Fourier Transform (WFT) and Wavelet Transform (WT).

Phase Measurement Profilometry (PMP) was first proposed by Srinivasan et al. [11]. The idea of this technique is to create a set of sinusoidal patterns which are projected and shifted over time. Every projection is shifted from the previous projection by a factor of $2\pi/N$, being N the total number of projections. The imaged sinusoidal patterns are deformed by the object surface, thus holding information about its 3D shape. It is important to mention that this algorithm requires a minimum of $N=3$ pattern projections to correctly extract the phase deviation (here phase deviation refers to the deformation caused by the object shape to the original phase). The projected patterns are therefore of the form:

$$I_n^p(y^p) = A^p + B^p \cos(2\pi f \cdot y^p - 2\pi n / N) \quad (1)$$

where A^p and B^p are the projection constants, f the spatial frequency of the fringes and y^p the coding axis, $n=0, 1, \dots, N-1$ is the shifting value, the index p refers to the projected pattern. The imaged intensity values of the measured object, once the set of patterns is projected is:

$$I_n(x, y) = \alpha(x, y) [A + B \cos(2\pi f y^p + \phi(x, y) - 2\pi n / N)] \quad (2)$$

where $\alpha(x, y)$ is the different albedo and $\phi(x, y)$ represents the phase deviation introduced by the object shape. The phase deviation is extracted from the formula shown in Eq. (3), which cancels the effect of the different albedo.

$$2\pi f y^p + \phi(x, y) = \arctan \left[\frac{\sum_{n=1}^N I_n(x, y) \sin(2\pi n / N)}{\sum_{n=1}^N I_n(x, y) \cos(2\pi n / N)} \right] \quad (3)$$

From a minimum of three shifted patterns, it is possible to create a relative phase map and to extract the phase deviation caused by the object shape. However, under real conditions, many more patterns are required [12], limiting the applications only to static scenes.

Fourier Transform (FT) came to cope with the limitation of PMP to static scenes. FT employs the frequency domain to suppress the background component of the imaged pattern. Therefore, one single projection is enough to suppress the albedo and extract the phase

deviation. FT was first proposed by Takeda and Mutoh [13], and different variations have been proposed since then [14–16]. The received signal (Eq. (2)) is first filtered in frequency and then the phase can be extracted, as shown in Eq. (4) and Eq. (6):

$$I(x, y) = a(x, y) + c(x, y)e^{2\pi i f y} + c^*(x, y)e^{-2\pi i f y} \quad (4)$$

where

$$c(x, y) = \frac{1}{2} b(x, y) e^{i\phi(x, y)} \quad (5)$$

and $c^*(x, y)$ is the conjugated value of $c(x, y)$. Finally, the phase component $\phi(x, y)$ is extracted from the imaginary part of Eq. (6):

$$\log[c(x, y)] = \log \left[\left(\frac{1}{2} \right) b(x, y) \right] + i\phi(x, y). \quad (6)$$

The relative phase map $\phi(x, y)$ can be then used as an input to a proper phase unwrapping algorithm. Some FT techniques have been implemented using 2D Fourier decomposition, which provides better separation of phase and noise when dealing with coarse objects [17]. However, most of the sources of noise come from the non-spatial stationarity of the images. Theoretically speaking, Fourier decomposition performs optimally with stationary signals, which is not the case in pattern analysis. As a consequence of their limited spatial dimensions, the projected patterns suffer from intensity changes due to surface discontinuities. This causes the frequency harmonics to interfere with the first frequency harmonic, making impossible to extract the frequencies around the first harmonic without errors. The albedo can also interfere with the first harmonic. These effects are known as leakage distortion, and it manifests itself in the form of large errors at the borders of the extracted phase map and wrong reconstruction of areas around holes in the fringe pattern.

The Spatial Phase Detection (SPD) constitutes an alternative to FT. This method was initially proposed by Toyooka and Iwaasa [18], and represents an alternative to FT in the spatial domain. The analysis of the received signal (Eq. (7)) is done using the sine and cosine functions, as can be observed in Eq. (8), Eq. (11):

$$I(x, y) = \alpha(x, y) [A + B \cos(2\pi f y^p + \phi(x, y))] \quad (7)$$

$$\begin{aligned} I_c(x, y) &= \alpha(x, y) [A + B \cos(2\pi f y^p + \phi(x, y))] \cdot \cos(2\pi f y^p) \\ &= \alpha(x, y) \cdot A \cos(2\pi f y^p) + \frac{1}{2} \alpha(x, y) \cdot B \cos(4\pi f y^p) + \frac{1}{2} \alpha(x, y) \cdot B \cos(\phi(x, y)) \end{aligned} \quad (8-10)$$

$$\begin{aligned} I_s(x, y) &= \alpha(x, y) [A + B \cos(2\pi f y^p + \phi(x, y))] \cdot \sin(2\pi f y^p) \\ &= \alpha(x, y) \cdot A \sin(2\pi f y^p) + \frac{1}{2} \alpha(x, y) \cdot B \sin(4\pi f y^p) - \frac{1}{2} \alpha(x, y) \cdot B \sin(\phi(x, y)) \end{aligned} \quad (11-13)$$

Now $\phi(x, y)$ varies much more slowly than any terms containing f and so only the last term in each new function is a low-frequency term. This part of the function can then be extracted by low-pass filtering. Regarding the Euler's formula for the sine and cosine functions and the principles of Fourier Transform applied on sinusoidal functions [19], this step provides similar results than obtaining the real and the imaginary components of the Fourier Transform applied to the incoming signal. Therefore, the last step is to extract the phase component from these components, which is obtained by applying the arctangent function (Eq. (14)):

$$\phi(x, y) = \arctan \left[\frac{r(x, y) * I_s(x, y)}{r(x, y) * I_c(x, y)} \right] \quad (14)$$

where $r(x,y)$ represents a low-pass filter, and $*$ denotes convolution. It is important to note that Toyooka and Iwaasa use integration to extract the phase terms, whereas other authors using related spatial domain methods apply different low-pass filters [20]. As in FT, this method suffers from leakage distortion when working with fringe patterns, as no local analysis is performed to avoid spreading errors due to discontinuities and different albedo.

The Windowed Fourier Transform (WFT) was proposed to solve the leakage distortion problem. The idea is to window and split the signal into segments before the analysis in frequency domain is performed. The received signal is filtered applying the WFT analysis transform shown in Eqs. (15) and (17)

$$Sf(u, v, \xi, \eta) = \int_{-\infty}^{\infty} \int_{-\infty}^{\infty} f(x, y) \cdot g(x-u, y-v) \cdot \exp(-j\xi x - j\eta y) dx dy \quad (15)$$

being (x,y) , (ξ,η) the translation and frequency coordinates respectively, and $g(x,y)$ the windowing function. When $g(x,y)$ is a Gaussian window, the WFT is called a Gabor transform; that is:

$$g(x, y) = \frac{1}{\sqrt{\pi\sigma_x\sigma_y}} \cdot \exp\left(-\frac{x^2}{2\sigma_x^2} - \frac{y^2}{2\sigma_y^2}\right) \quad (16)$$

where σ_x and σ_y are the standard deviations of the Gaussian function in x and y , respectively. Eq. (15) provides the 4-D coefficients $Sf(u, v, \xi, \eta)$ corresponding to the 2D input image. The windowing permits the WFT to provide frequency information of a limited region around each pixel. The Gaussian window is often chosen as it provides the smallest Heisenberg box [21]. Once the 4D coefficients are computed, the phase can be extracted. There are two main techniques for phase extraction in WFT: Windowed Fourier Filtering (WFF) and Windowed Fourier Ridge (WFR). In WFF the 4D coefficients are first filtered, suppressing the small coefficients (in terms of its amplitude) that correspond to noise effects.

The inverse WFT is then applied to obtain a smooth image:

$$f(\bar{x}, y) = \int_{-\infty}^{\infty} \int_{-\infty}^{\infty} \int_{-\eta_1}^{\eta_1} \int_{-\xi_1}^{\xi_1} Sf(u, v, \xi, \eta) \cdot g_{u,v,\xi,\eta}(x, y) d\xi d\eta du dv \quad (17)$$

where:

$$Sf(u, v, \xi, \eta) = \begin{cases} Sf(u, v, \xi, \eta) & \text{if } |Sf(u, v, \xi, \eta)| > \text{threshold} \\ 0 & \text{if } |Sf(u, v, \xi, \eta)| < \text{threshold} \end{cases} \quad (18)$$

The estimated frequencies $\omega_x(x,y)$ and $\omega_y(x,y)$ and corresponding phase distribution is obtained from the angle given by the filtered WFF, as explained in [21]. In WFR, however, the estimated frequencies are extracted from the maximum of the spectrum amplitude, as shown in Eq. (19)

$$[\omega_x(u, v), \omega_y(u, v)] = \operatorname{argmax}_{\xi, \eta} |Sf(u, v, \xi, \eta)| \quad (19)$$

The phase can be directly obtained from the angle of the spectrum for those frequency values selected by the WFR (phase from ridges), or integrating the frequencies (phase by integration). Phase from ridges represents a better solution than phase from integration (despite some phase correction may need to be applied [21]), as in phase from integration errors are accumulated and lead to large phase deviations. It is important to note the importance of setting a proper window size, independently of the phase extraction algorithm employed. The window size must be small enough to reduce the errors introduced by boundaries, holes and background illumination, at the same time it must be big enough to hold some periods and hence allow the detection of the main frequency to perform an optimal filtering. In applications where the frequency varies considerably during the analysis (in space or in time) this trade-off is difficult to achieve and noise arises due to a wrong frequency detection. Wavelet Transform (WT) was proposed to solve the aforementioned trade-off. In WT the window size increases when

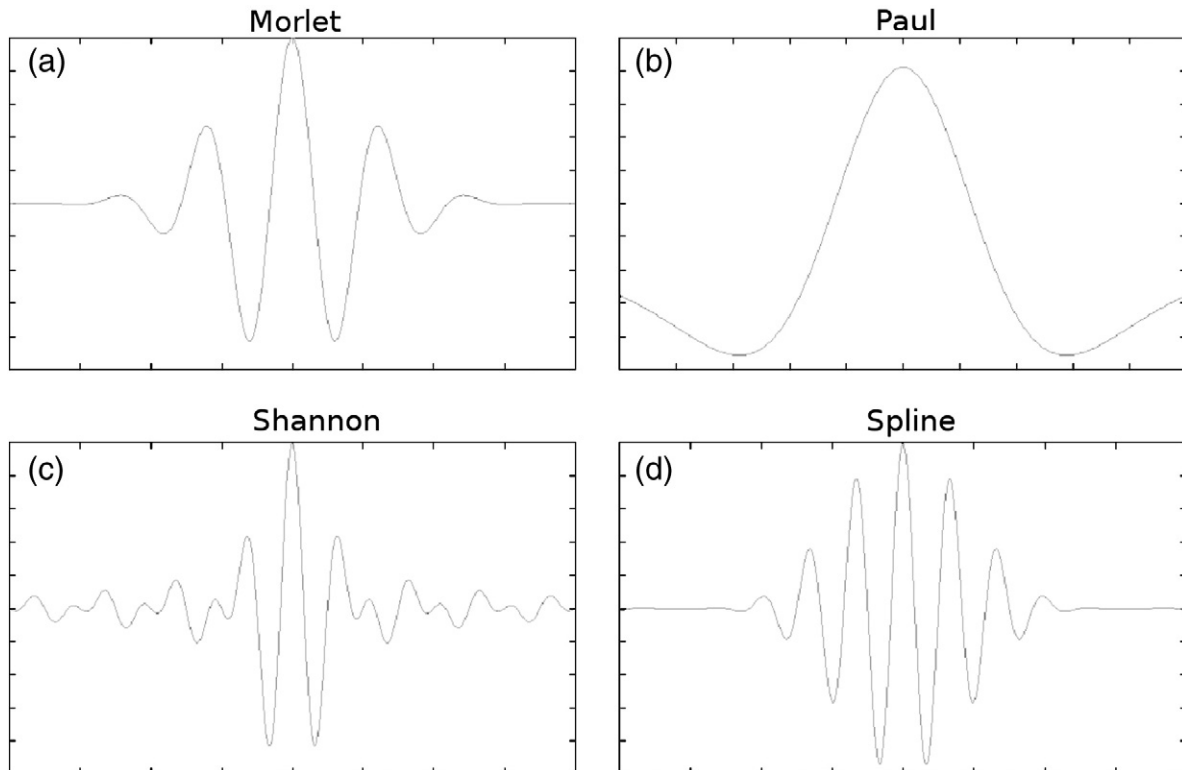


Fig. 1. Diagram of Morlet (a), Paul (b) Shannon (c) and Spline (d) wavelets, traditionally used in fringe pattern analysis.

the frequency to analyze decreases, and vice-versa. This allows to remove the background illumination and prevent the propagation of errors produced during the analysis, which remain confined in the corrupted regions alone [22]. Additionally the leakage effects are reduced, avoiding having large errors at the edges of the extracted phase maps. The Continuous Wavelet Transform (CWT) is a sub-family of WT that perform the transformation in the continuous domain. Moreover, it is common to use CWT with complex wavelets for the analysis of the fringe patterns [23]. The 1D-CWT algorithm analyzes the fringe pattern on a row by row basis, whereas the 2D-CWT algorithm is an extension of the analysis to the two dimensional space. In 2D analysis a 4D transform is obtained from WT (the daughter wavelets are obtained by translation, dilation and rotation of the previously selected mother wavelet). Once this is performed, phase extraction is pursued using the phase from ridges or the phase by integration algorithms, also named phase estimation and frequency estimation (similarly to WFT). As in WFT, it has been proven that the phase from ridges provides better results than the phase from integration, due to the accumulative effect in the phase from integration algorithm [23]. Another characteristic of WT is that the window size increases when the horizontal or vertical fringe frequencies decrease. This can be a troublesome for the analysis of some fringe patterns where the carrier frequency is extremely low or high [24]. Moreover, in computational applications a dyadic net is used to generate the set of wavelet functions. That is, the size of the wavelet is modified by the factor 2^j . This can lead to some problems in applications like fringe patterns analysis, where the change in the spatial fringes frequencies throughout the image is not high enough to produce a relative variance of 2^j in the size of the optimal wavelet.

3. WFT versus WT

In order to analyze the pros and cons of WFT and WT techniques applied to fringe pattern analysis, a theoretical and a practical comparison is required. The main difference between both techniques is the way the window size is set, depending on whether they have a fixed or a variable value. As stated in [25], WT performs better with signals having a wide range of frequencies with shorter correlation times for the higher frequencies than for the lower frequencies. This is the case in natural scenes, where low-frequency components usually last for longer durations than high-frequency components. However, in fringe patterns their periodicity and spatial extension does not depend on the selected frequency. Nevertheless, they mostly present spatial-harmonic components around the selected frequency. This is the reason why, despite many authors claim the goodness of WFT [22,23], there are some recent works that state the best suitability of WFT [21,26]. Another point to consider is the resistance to noise. It has been demonstrated [26] that for noiseless fringe patterns the frequency components can be accurately recovered in either small or large windows, regardless the frequency value. However, under the presence of higher noise on the imaged fringe pattern, an optimal selection of the window size reveals crucial for filtering the noise while preserving the main frequency components. Under these circumstances, the fixed window size of WFT performs better than the variable window size of WT. This is mainly due to the dyadic net used in practical applications of WT. This net changes geometrically (by two) the window size for adjacent levels of dilation, being excessive for some applications where the main frequency stands close to a fixed value (like in fringe pattern analysis).

Another point to consider is the importance of selecting a window having good localization in both frequency and space, in order to perform an optimal analysis of the fringe pattern. In WT, the mother wavelet signals usually used in fringe pattern analysis are, among others, the Morlet wavelet, the Paul wavelet, the Shannon wavelet and Spline wavelet [27–30]. All of them use a low-pass envelope signal modulating a frequency sinusoidal signal, thus presenting good localization in time and frequency. In WFT, the Gabor transform has

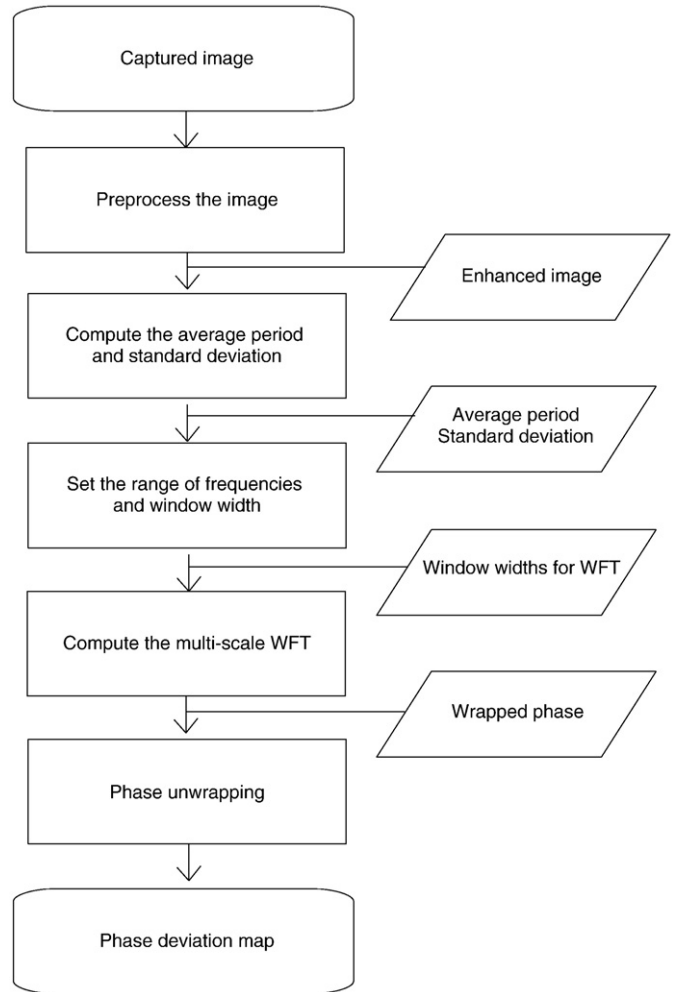


Fig. 2. Diagram of the proposed algorithm showing the required steps.

been traditionally used in fringe pattern analysis, as it provides the smallest Heisenberg box [31,32]. However, is not possible to find in the literature a study of windowing signals assuring good results for fringe pattern analysis using WFT. As this work has been already done in WT [23], it is recommended to adapt those optimal mother wavelets to WFT. This would permit a fair comparison between both techniques.

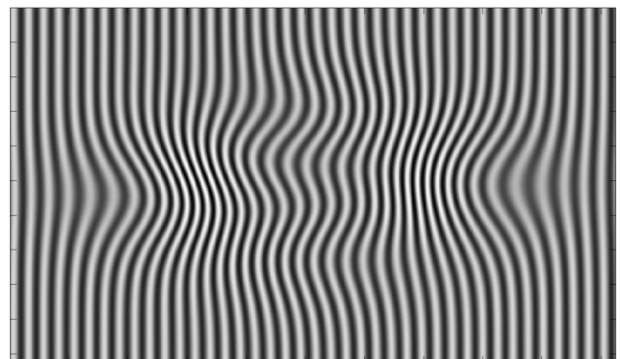


Fig. 3. Peak function used as the input image, containing phase variation at different speeds, and added noise.

3.1. Adaption of the wavelet signals to the use in WFT

The suitability of some mother wavelets for fringe pattern analysis in WT has been outlined in [22–24]. The best situation is given when the signal presents good localization in both space and frequency; that is, presenting some zeros at infinite (low pass shape). This is achieved by some mother wavelets like the Morlet, the Paul, the Shannon and the Spline wavelet (Fig. 1 and Eqs. (20–23)). Among them, the Paul wavelet has the best time localization capability, but at the same time it has the worst frequency localization [27]. This makes the Paul

mother wavelet the more suitable for demodulating fringe patterns that exhibit high signal to noise ratio and rapid phase variations. Besides, the Morlet wavelet presents a Gaussian shape and thus has better localization in the frequency domain than the Paul wavelet. Therefore, it is more suitable for demodulating fringe patterns with slow phase variations and low signal to noise ratios.

$$\Psi_{\text{Morlet}}(x) = \frac{1}{(f_b^2 \pi)^{1/4}} \exp(2\pi i f_c x) \cdot \exp\left(\frac{-x^2}{2f_b^2}\right) \quad (20)$$

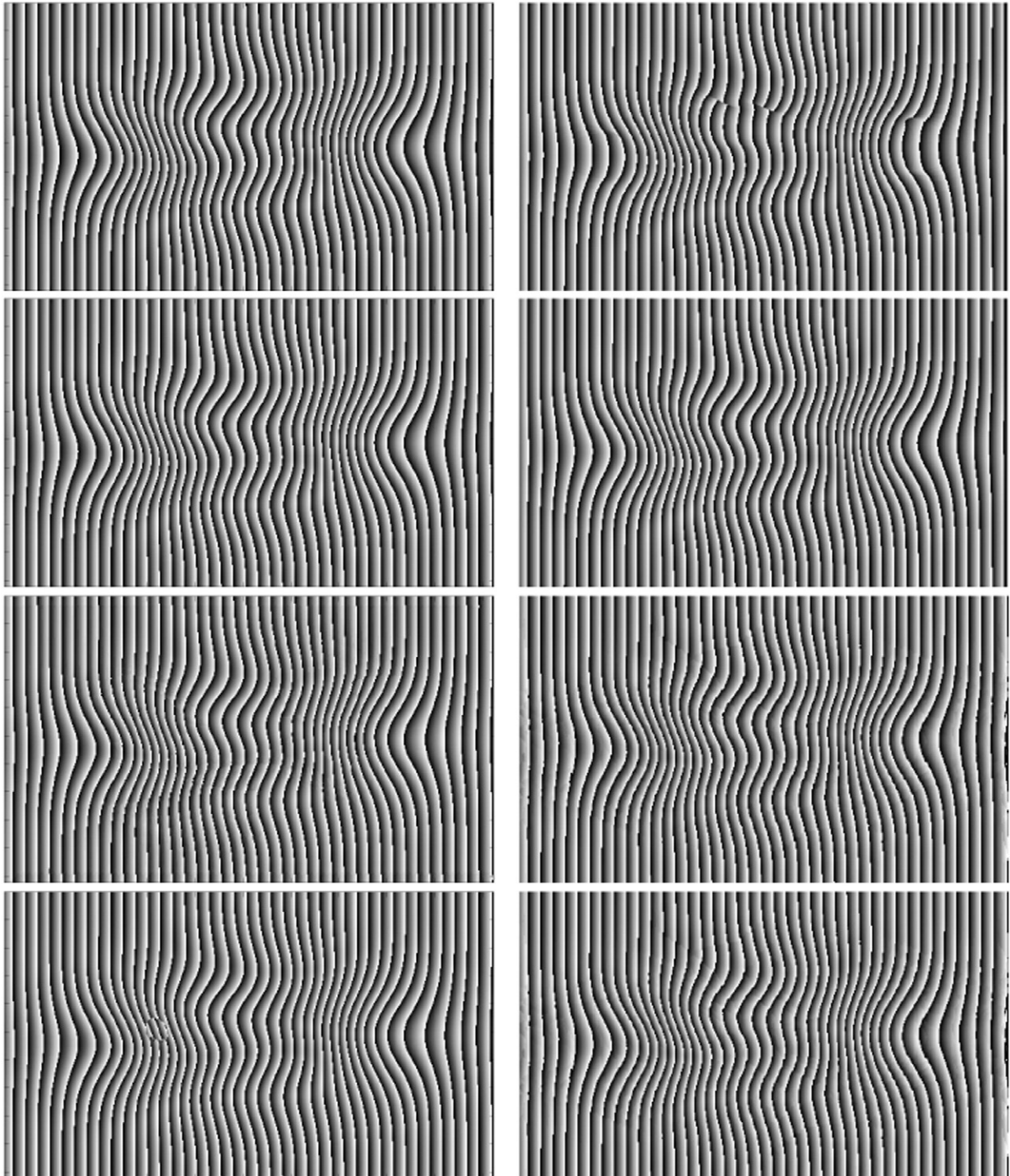


Fig. 4. Simulation results of the wrapped phase (from $-\pi$ to π): on the left column the four adapted mother wavelets (Morlet, Paul, Shannon, and Spline). On the right column, their corresponding results in WT.

Table 1
Relative mean error of the recovered phase.

Error (%)	Morlet	Paul	Shannon	Spline
WFT	0.073	0.058	0.156	0.169
WT	0.115	0.067	0.162	0.174

$$\Psi_{Paul}(x) = \frac{2^n n! (1-ix)^{(n+1)}}{2\pi \sqrt{\frac{(2n)!}{2}}} \quad (21)$$

$$\Psi_{Shannon}(x) = \sqrt{f_b} \exp(2\pi i f_c x) \sin c(f_b x) \quad (22)$$

$$\Psi_{b-spline}(x) = \sqrt{f_b} \exp(2\pi i f_c x) \left[\sin c\left(\frac{f_b x}{m}\right) \right]^m \quad (23)$$

where n is the order of the Paul mother wavelet, f_c is the mother wavelet central frequency, f_b is the variance of the window and m is an integer value that determines the Spline wavelet. The selected mother wavelets have been adapted to the use in the multiresolution WFT algorithm proposed in these lines. It must be mentioned that all of them contain a modulated sinusoidal frequency in its definition. Making a comparison with WFT (Eq. (15)), this would correspond to the exponential modulating frequency employed. Therefore, the window of the WFT is equivalent to the shape of the selected mother wavelet. The introduction of a sinusoidal frequency becomes necessary when it is not implicitly contained in the wavelet definition. Another point to take into account is the normalization of the adapted wavelet signals, as a change in the window size must be compensated by an increment of the modulus of the signal, to preserve the value of energy provided by the WFT algorithm. Finally, it must be considered the ability to adapt the size of the wave envelope relative to the wave period for many mother wavelet functions (Morlet, Shannon, and Spline). In wavelet analysis, this parameter is used to create a set of complex mother wavelets within the same wavelet family. In WFT this is equivalent to just changing the size of the window, as the preset frequency does not change with this size.

4. Algorithm for the automatic selection of the window

Given the signal in the form $f(x) = a(x,y) + b(x,y) \cdot \cos[\phi(x,y)]$, the accuracy of the retrieved phase is directly linked to the size of the window, the signal envelope and its behavior in frequency domain. Hence, an algorithm to set the optimal window for any WFT signal and for any fringe pattern reveals to be necessary. Regarding this point, recently Li and Yang [33] proposed a two-step algorithm to determine

locally, among a set of patches, the most likely window size for WFT. First, the instantaneous frequencies on x and y direction of the modulated fringe pattern are determined by two-dimensional Gabor Wavelet Transform (2D-GWT) [34] and, then the local stationary lengths are obtained. Furthermore the so-called Two-dimensional Multiscale Windowed Fourier Transform (2D-MWFT) was applied. This algorithm applied local two-dimensional Gaussian windows, and is performed for each section of the modulated fringe pattern to achieve multiresolution analysis and phase demodulation. Despite the computational cost associated to the two frequency transformations required in this technique, quite good results are obtained as can be observed in [33]. In our work a new proposal for the automatic setting of the window size is done. The proposed algorithm is executed in only one WFT step, taking into account the uncertainty of the received image.

The proposed algorithm is depicted in Fig. 2, and described in the following section, emphasizing the steps that permit the automatic detection of the window size.

4.1. Preprocessing the image

The preprocessing step consists on a salt and pepper filtering and a histogram equalization. This reduces the noise present in the captured image and enhances the image contrast for a latter frequency component extraction. Finally, a DC filter is applied to extract the DC component of the image. This step delivers an enhanced image where the fringes are perceived more clearly.

4.2. Setting the average period and the standard deviation

This step represents the main idea of the automatic selection of the window. The algorithm extracts an approximated value of the number of periods existing in every line along the coding axis, of the image. To do so, a local maximum extraction is performed for the both maximum and the minimum values in every line along the coding axis. The algorithm avoids false positive by suppressing those local maximum that are not followed by a local minimum. Once the number of periods is extracted for every image column, an average of the global period, the corresponding frequency and its variance are computed. This variance represents the uncertainty in the estimated frequency, and is crucial to perform a global analysis of the image. Regarding this point a discussion about whether the selection of global or local variance for patches in the image is required. In principle, a local selection seems to be more appropriate as it can distinguish frequencies of different patches. However, it requires more computation as the WFT must be applied in every patch. Using a global WFT and the appropriate range for the analytic frequencies, a trade-off to delete noisy frequencies and to preserve the ones related

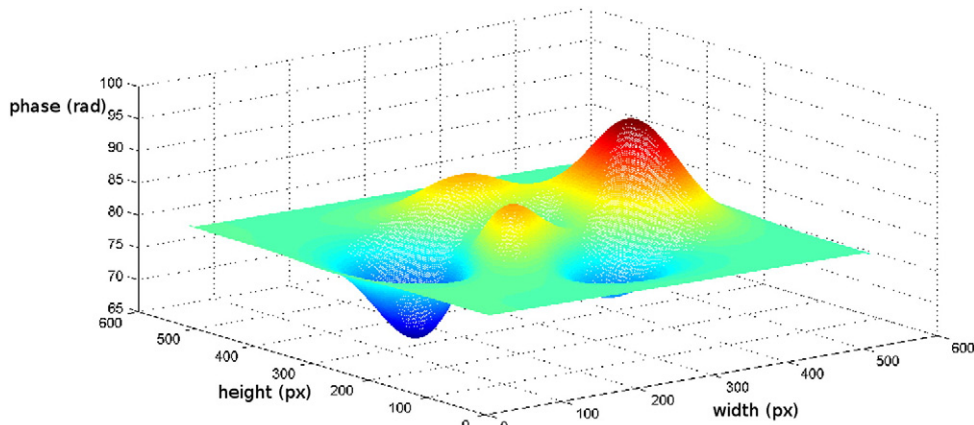


Fig. 5. Recovered unwrapped phase, in radians, for the simulated input fringe pattern of Fig. 3. Morlet WFT has been used.

to the real shape must be set. This reduces to just one of the total number of WFT, thus reducing the computational time.

4.3. Setting the range of frequencies and the window

The selection of the appropriate range of frequencies is done according to the variance and the average values of the period. For instance, considering the range $[f_m - 3 \cdot \text{std}(f), f_m + 3 \cdot \text{std}(f)]$ in both x and y axes, the 95% of detected frequencies are analyzed, according to the Central Limit Theorem [35]. The frequencies outbounding this range are considered outliers. In practice, this range can be reduced to $[f_m - 2 \cdot \text{std}(f), f_m + 2 \cdot \text{std}(f)]$ (90% of the frequencies are represented) without a significant lose in accuracy. Another variable to consider is the window size related to the number of periods of the sinusoidal signal. In contrast to the mother wavelets in WT, WFT does not require the number of periods to be linked to the sinusoidal oscillation of the signal. In WT the number of periods determines a mother wavelet within the same wavelet family, and usually goes from one up to three or four periods, allowing to hold information about the frequency without losing local information. In WFT though, the number of periods can be directly set from the definition of the signal. In our algorithm it has been tested from one up to

three periods, determining the optimal value by the ridge extraction algorithm (WFR).

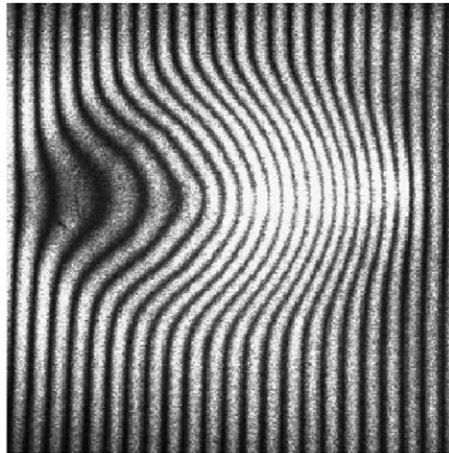
4.4. Computing the WFT

Once all the parameters are defined, the set of signals having different sinusoidal frequencies and windows are convolved with the enhanced image. As a result, a 4D matrix is obtained (having dimensions of x and y axes, window size and frequency). The WFR algorithm is then applied to compute the most likely values of window, w_x , w_y , and the corresponding phase value, delivering the wrapped phase in the interval $[-\pi, \pi]$.

4.5. Phase unwrapping

In order to obtain the unwrapped phase and compute the phase difference with the projected pattern, a phase unwrapping algorithm must be applied. To this end, we use the algorithm of Herraiz et al. [36]. This algorithm performs a phase unwrapping based on sorting by reliability following a non-continuous path. As stated in [36], the algorithm is suitable for fringe analysis as it minimizes the effects of the noise present in the wrapped phase and provides robust results

(a) Input image



(b) Unwrapped phase map

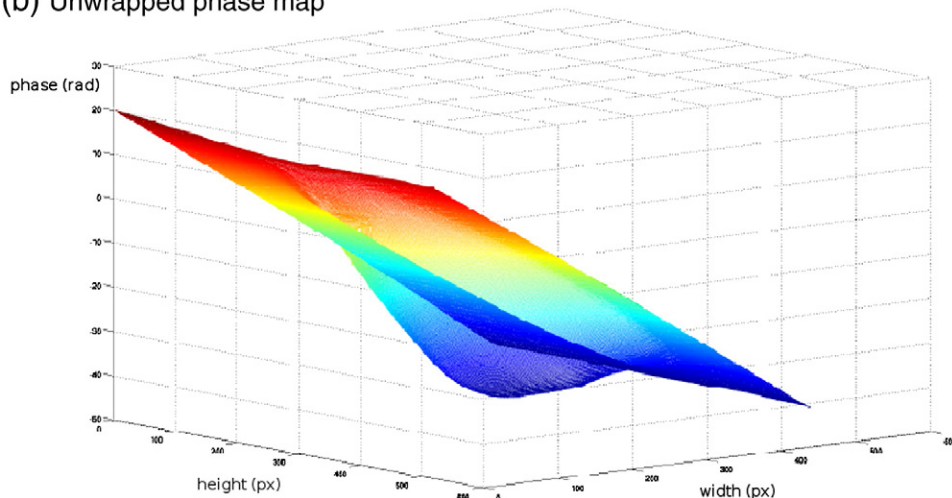


Fig. 6. Input image and reconstructed unwrapped phase map in radians (using Paul wavelet for WFT).

under presence of slopes (although errors can still arise in some specific discontinuities due to the periodicity of the pattern).

5. Results

The proposed algorithm has been tested in both simulated and real conditions. The setup used for the real tests was composed of an LCD video projector (Epson EMP-400 W) with a resolution of 1024×768 pixels and a camera (Sony 3CCD) digitizing images of

size 512×512 in monochrome. All the algorithms were programmed on MATLAB and executed on a standard Intel Core2 Duo CPU at 3.00 GHz.

5.1. Simulated results

The proposed algorithm was tested using simulated data. The peak function available in Matlab has been considered in the test, since it has become a benchmark for fringe pattern analysis, as stated in [23]

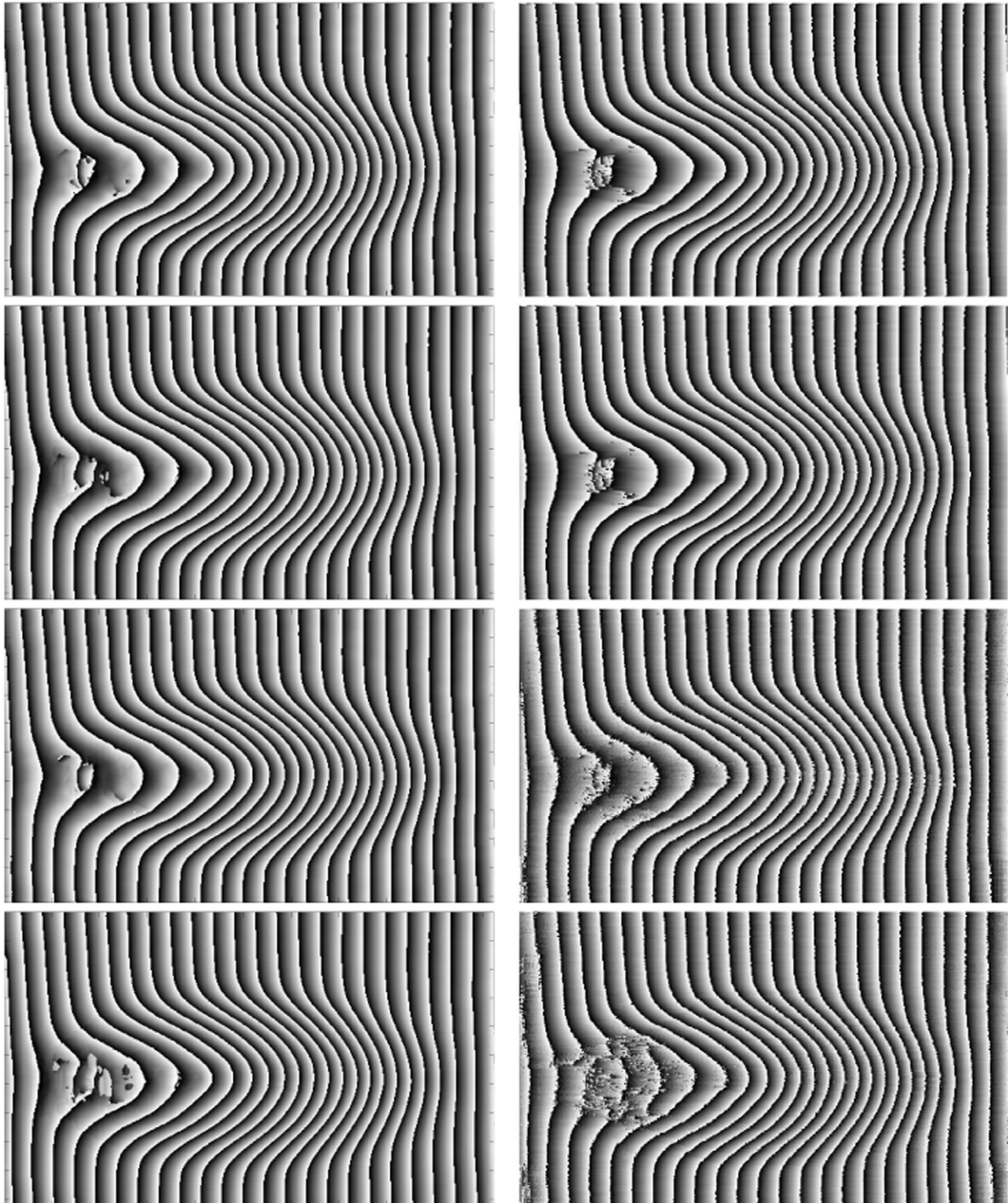


Fig. 7. Plastic bended sheet: on the left column, experimental results for the four adapted mother wavelets (Morlet, Paul, Shannon, and Spline). On the right column, their corresponding results in WT.

(Fig. 3). The peak function presents different levels of deformations, therefore it is optimal for analyzing the performance of the adapted signals under different 3D shapes. Some blurring was performed to the image to simulate the noise introduced by the projector-camera pair (Fig. 3). In addition, the peak function was also analyzed using the WT (specifically the 2D-CWT) in order to compare the performance of both techniques. The results of the wrapped recovered phase are shown in Fig. 4.

As can be observed in Fig. 4, the best performance of WFT was obtained using the adapted Morlet wavelet and the adapted Paul wavelet. Both wavelets present a clear free of artifacts wrapped phase image. Moreover, the boundaries have been recovered optimally. Worse results are obtained with the adapted Spline wavelet (with $m=2$), as the change in its envelope signal does not suit optimally with the fringe pattern sinusoidal shape. Phase errors are also present across all the image for the analysis using the adapted Shannon wavelet, which actually is the Spline wavelet with $m=1$. Looking at the wrapped phase obtained using the Wavelet Transform, we observe how the errors presented in WFT also appear in WT. This enforces the idea that Morlet and Paul wavelets are more suitable for fringe pattern analysis than Shannon and Spline wavelets. Moreover, we can appreciate some errors in the image corner for the case of the Shannon and the Spline wavelet analyses, not present with the WFT phase extraction algorithm proposed in this work. Table 1 provides some quantitative results of the previous recovered phases compared to the input phase, where the relative mean error represents the mean

of the sum of the absolute error between the computed wrapped phase map and the input phase map. Finally, as example of the reconstruction results, the unwrapped phase map of the Morlet WFT is shown in Fig. 5.

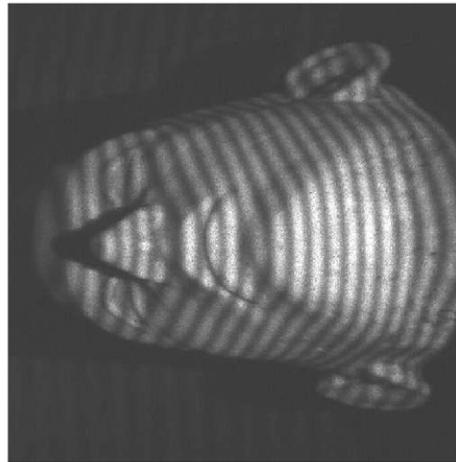
5.2. Experimental results

This section analyzes the performance of the proposed algorithm reconstructing two different objects. The first is a plastic lambertian sheet having a smooth surface with an irregular deformation in the middle of the object. The second object is a ceramic lambertian human face. The proposed technique is applied and the corresponding wrapped phase maps are compared. The unwrapping algorithm developed by Herraes et al. [36] is employed to extract the unwrapped phase map of the objects. The input images and their corresponding unwrapped phase maps are shown in Figs. 6 and 8, respectively. The wrapped phase maps corresponding to either the output of the WFT or WT (specifically the 2D-CWT) are analyzed in detail hereafter.

5.2.1. Plastic sheet

The Morlet and the Paul wavelets suffer from larger error than the respective signals in WFT, as can be observed in Fig. 7. The errors are located in the region having larger variation in depth. The wavelet analysis introduces some doubled frequency components due to the effect of the dyadic net in the phase estimation. This does not happen in WFT, where the discrepancy to the correct phase is lower. The same

(a) Input image



(b) Unwrapped phase map

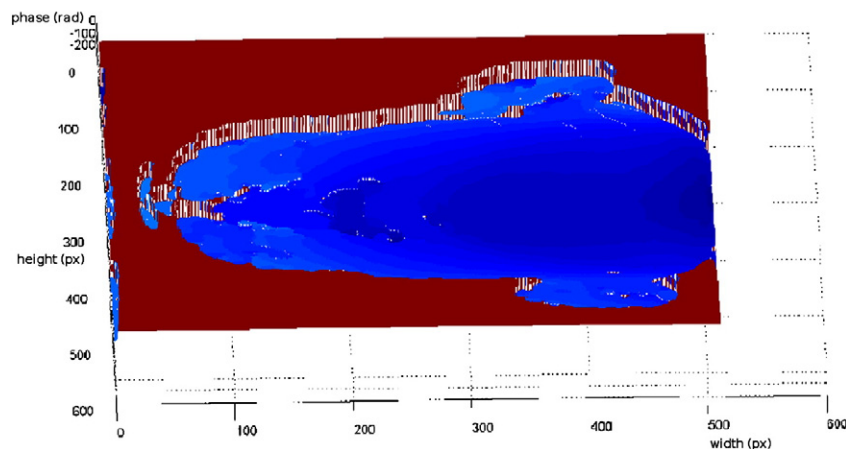


Fig. 8. Input image and reconstructed unwrapped phase map in radians (using Paul wavelet for WFT).

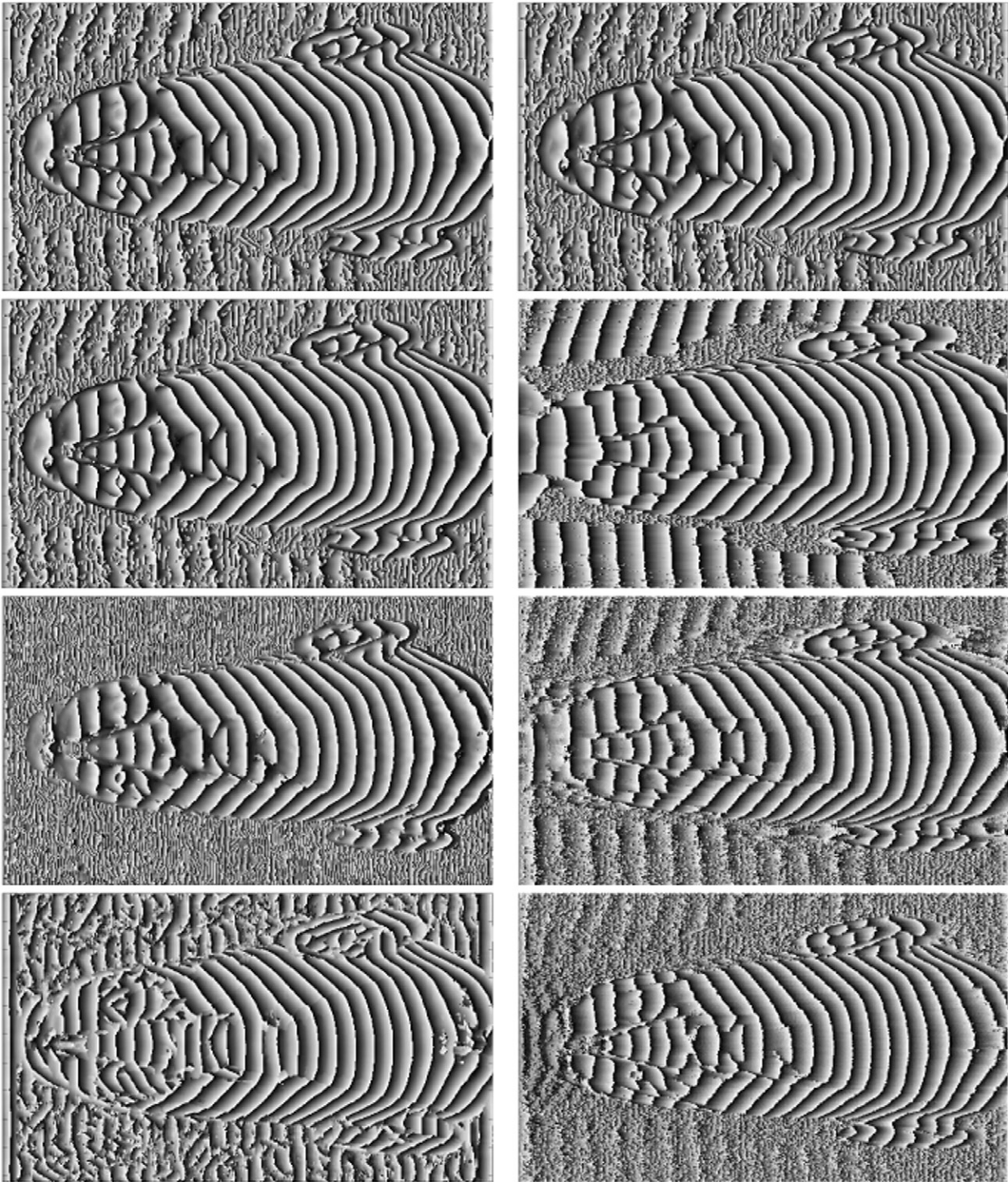


Fig. 9. Ceramic human face: on the left column, experimental results for the wrapped phase (from $-\pi$ to π) of the four adapted mother wavelets (Morlet, Paul, Shannon, and Spline). On the right column, their corresponding results in WT.

errors are present in the Shannon WT mode. The Shannon WFT, however, performs optimally for this image. Increasing the value of m up to $m=2$, though (in fact the Spline function with $m=2$) errors arise in some region of the captured image. Therefore, Morlet, Paul and Shannon WFT techniques perform optimally in this case.

5.2.2. Ceramic human face

Phase estimation has been pursued for the four wavelet signals in both WT and WFT. The results are shown in Fig. 9. Best results are

obtained for the Morlet signal, as in the previous images. Among them, the WFT performs better than WT in presence of slopes, as can be noise near the nose and the eyes.

6. Conclusions

Continuous coding strategies represent an important field of research in CSL. In these approaches, the depth of a given point in the image is determined by the deviation of its gray value with respect to the

projected pattern. Among them, Fourier Transform, Windowed Fourier Transform and Wavelet Transform techniques were proposed to work in dynamic scenarios, as a single projection is permitted. All these techniques make use of the frequency domain to extract the principal components of the image and compute its phase deviation map, from which the unwrapped phase map can be extracted. It has been tested that for fringe pattern analysis, the windowed transform techniques (WFT and WT) perform better than the global transformation FT, as the frequency components of a given region remain close to that region [23,27]. Following the idea of Li and Yang [33], an automatic and fast window size detection algorithm has been proposed in this paper. This algorithm performs a fine tuning of the window. First, this algorithm extracts the global average and the standard deviation of the frequency components present in the image. Posteriorly, a frequency analysis is done for the components representing the 95% of the frequency range, though this percentage can be modified. Moreover, in order to perform a fair comparison between WFT and WT, the traditional mother wavelets used for WT analysis have been adapted to WFT. For the phase extraction, the maximum ridge algorithm has been used [21]. Finally, the phase unwrapping algorithm of [36] is employed to compute the unwrapped phase map from the wrapped phase. The results show how the WFT with automatic window size detection performs better compared to the traditional WT technique. This is mainly due to the nature of the dyadic net used in WT, which scales the window by a factor of 2^j between adjacent size values. The proposed WFT, however, performs a fine tune of the window size between a set of values around the optimal size corresponding to the global frequency average. Some simulated and real results have been obtained. In simulated data the Morlet and Paul wavelets show better performance than the Shannon and the Spline wavelets, thanks to the greater similarity of its signal shape to the sinusoidal nature of the fringe pattern. This fact is also noticed in the real experiments. A plastic curved sheet and a ceramic human face were imaged, and the wrapped phase map was obtained for the four mother wavelets considered for the analysis. Similarly to the simulations, WFT performs better than WT, showing the best performance for the Morlet and the Paul mother wavelets. This proves that the use of an adapted Paul or Morlet mother wavelet to the use in WFT is optimal when the window size is set properly. The fine tuning provided by the automatic window selection algorithm assures an optimal selection of the local frequency thus minimizing the error in the recovered phase map dealing to more accurate 3D reconstructions.

Acknowledgments

This work is supported by the research MCINN project DPI2007-66796-C03-02 of the Spanish Ministry of Science and Innovation. S. Fernandez-Navarro is supported by the Spanish government scholarship FPU.

References

- [1] P.S. Huang, S. Zhang, F.P. Chiang, et al., *Optical Engineering* 44 (2005) 142.
- [2] A.K.C. Wong, P. Niu, X. He, *Computer Vision and Image Understanding* 98 (3) (2005) 398.
- [3] J. Salvi, J. Batlle, E. Mouaddib, *Pattern Recognition Letters* 19 (11) (1998) 1055.
- [4] F. Forster, A high-resolution and high accuracy real-time 3D sensor based on structured light, Proc.3th International Symposium on 3D Data Processing, Visualization, and Transmission, 2006, p. 208.
- [5] R.A. Morano, C. Ozturk, R. Conn, S. Dubin, S. Zietz, J. Nissano, *IEEE Transactions on Pattern Analysis and Machine Intelligence* 20 (3) (1998) 322.
- [6] J. Pages, J. Salvi, C. Collewet, J. Forest, *Image and Vision Computing* 23 (2005) 707.
- [7] B. Carrhill, R. Hummel, *Computer Vision, Graphics, and Image Processing* 32 (3) (1985) 337.
- [8] J. Tajima, M. Iwakawa, 3-D data acquisition by rainbow range finder, *Pattern Recognition*, 1990. Proceedings., 10th International Conference on, vol. 1, 1990, p. 309.
- [9] J. Salvi, S. Fernandez, T. Pribanic, X. Llado, *Pattern Recognition* 43 (8) (2010) 2666.
- [10] J. Salvi, J. Pages, J. Batlle, *Pattern Recognition* 37 (4) (2004) 827.
- [11] V. Srinivasan, H.C. Liu, M. Haliou, *Applied Optics* 24 (1985) 185.
- [12] T. Pribanic, H. Dapo, J. Salvi, Efficient and low-cost 3D structured light system based on a modified number-theoretic approach. *EURASIP Journal of Advances in Signal Processing*, Hindawi Publishing Corporation, 2010.
- [13] M.T.K. Takeda, M. Mutoh, *Applied Optics* 22 (1983) 3977.
- [14] J. Li, X. Su, L. Guo, *Optical Engineering* 29 (12) (1990) 1439.
- [15] W. Chen, P. Bu, S. Zheng, X. Su, *Optics & Laser Technology* 39 (4) (2007) 821.
- [16] H.M. Yue, X.Y. Su, Y.Z. Liu, *Optics & Laser Technology* 39 (6) (2007) 1170.
- [17] J.F. Lin, X. Su, *Optical Engineering* 34 (1995) 3297.
- [18] Y. Iwaasa, S. Toyooka, *Applied Optics* 25 (10) (1986) 1630.
- [19] J.G. Proakis, D.G. Manolakis, D.G. Manolakis, J.G. Proakis, *Digital Signal Processing: Principles, Algorithms, and Applications*, vol. 3, Prentice Hall, New Jersey, 1996.
- [20] F. Berryman, P. Pynsent, J. Cubillo, *Optics and Lasers in Engineering* 39 (1) (2003) 35.
- [21] Q. Kemao, *Optics and Lasers in Engineering* 45 (2) (2007) 304.
- [22] M.A. Gdeisat, D.R. Burton, M.J. Lalor, *Optics Communications* 266 (2) (2006) 482.
- [23] Abdulbasit Zaid Ahmed Abid, *Fringe Pattern Analysis using Wavelet Transforms*, PhD thesis.
- [24] Q. Kemao, *Applied Optics* 43 (17) (2004) 3472.
- [25] A.F. Laine, *Annual Review of Biomedical Engineering* (2) (2000) 511.
- [26] L. Huang, Q. Kemao, B. Pan, A.K. Asundi, *Optics and Lasers in Engineering* 48 (2) (2010) 141.
- [27] M.A. Gdeisat, A. Abid, D.R. Burton, M.J. Lalor, F. Lilley, C. Moore, M. Qudeisat, *Optics and Lasers in Engineering* 47 (12) (2009) 1348.
- [28] A. Dursun, Z. Saraç, H. Saraç Topkara, Phase recovery from interference fringes by using S-transform, *Measurement*, vol. 41 no. 4, Elsevier Ozder, S. and Necati Ecevit, F, 2008, pp. 403–411., issn=0263-2241.
- [29] M. Affi, A. Fassi-Fihri, M. Marjane, K. Nassim, M. Sidki, S. Rachafi, *Optics Communications* 211 (1–6) (2002) 47.
- [30] P. Tomassini, A. Giuliotti, L.A. Gizzi, M. Galimberti, D. Giuliotti, M. Borghesi, O. Willi, *Applied Optics* 40 (35) (2001) 6561.
- [31] Stephane Mallat, *A Wavelet Tour of Signal Processing*, AP Professional, London, 1997.
- [32] S. Qian, *Introduction to Time-frequency and Wavelet Transforms*, Prentice Hall PTR, 2002.
- [33] H. Li, C. Yang, Two-dimensional multiscale windowed Fourier transform based on two-dimensional wavelet transform for fringe pattern demodulation, *Optics & Laser Technology*, Elsevier (2010).
- [34] J. Weng, J. Zhong, C. Hu, *Applied Optics* 48 (18) (2009) 3308.
- [35] J.A. Rice, *Mathematical Statistics and Data Analysis*, Duxbury press Belmont, CA, 1995.
- [36] M.A. Herrez, J.G. Boticario, M.J. Lalor, D.R. Burton, *Applied Optics* 44 (7) (2005) 1129.